ACS Energy LETTERS

http://pubs.acs.org/journal/aelccp

LETTER

Interlayer-Tailored Alkyl-MXenes for Selective Electrochemical Lithium-Ion Extraction

Cansu Kök, Karamullah Eisawi, Jean G. A. Ruthes, Burcu Tan, Antje Quade, Michael Naguib, and Volker Presser*

Cite This: *ACS Energy Lett.* 2026, 11, 508–516

Read Online

ACCESS | Metrics & More | Article Recommendations | Supporting Information

ABSTRACT: **The efficient and selective extraction of lithium ions from aqueous media is crucial for resource recovery, yet remains challenging due to the chemical similarity of coexisting alkali ions, such as sodium. In this study, we report a two-step electrochemical strategy that utilizes tailored MXene electrodes for lithium ion extraction with enhanced selectivity and extraction rates. By preintercalating hexadecylamine (HDA) and decyltrimethylammonium (C10), which are long-chain organic molecules, into the $Ti_3C_2T_x$ MXene structure, we tailored the interlayer environment to favor lithium ions over sodium ions. The HDA-intercalated MXene demonstrated high Li^+/Na^+ selectivity with a lithium ion uptake of 2.2 mmol/L and a suppressed sodium ion uptake (<0.2 mmol/L). Extended cycling revealed that molecular preintercalation modulates ion transport pathways and influences structural and electrochemical stability. Both HDA-$Ti_3C_2T_x$ and C10-$Ti_3C_2T_x$ maintained a lithium ion purity of nearly 100% over 50 cycles.**

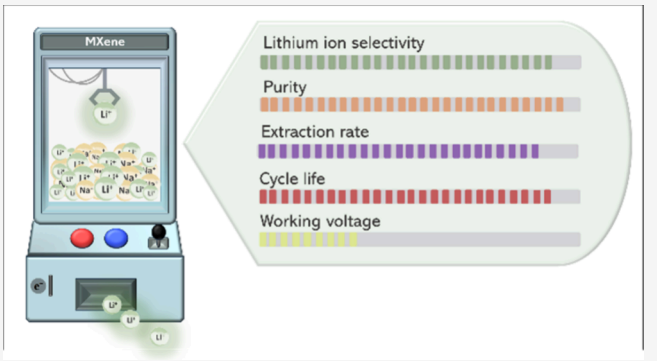

The increasing demand for lithium requires efficient and sustainable extraction technologies.[1] Conventional approaches, such as evaporation ponds and chemical precipitation, are limited by their inefficiency, high energy consumption, and environmental concerns.[2] As a promising alternative, electrochemical lithium ion separation offers high selectivity, low environmental impact, and scalability.[3−5] MXenes, which are two-dimensional transition metal carbides and nitrides, have attracted attention owing to their high electrical conductivity, surface chemistry tunability, and high affinity for cations.[6,7] Their layered structure with surface functional groups enables the precise tuning of their electrochemical properties for lithium-selective separation.[8,9] Furthermore, their high electrical conductivity ensures high charge/discharge rates with mechanical and chemical stability for prolonged electrochemical operations.[10] Recent studies have demonstrated the potential of MXenes in Li-selective electrosorption, revealing high capacity, fast kinetics, and high lithium ion diffusion mobility compared to traditional electrode materials.[11] Strategies such as doping, defect engineering, adjustable interlayer spacing, and composite formation with other nanomaterials can further enhance their lithium selectivity and durability, rendering MXenes a promising platform for sustainable extraction technologies.[12,13]

By modulating surface terminations, the interlayer spacing for ion sieving, and electronic characteristics, MXene-based electrodes can achieve enhanced lithium ion adsorption and desorption, thereby facilitating the selective separation of lithium ions from complex brine solutions.[14−17] For example, Chen et al.[8] developed a hybrid membrane by immobilizing a titanium-based lithium ion sieve (HTO) on a polyvinyl chloride (PVC) film and used MXene to enhance its adsorption sites. The resulting HTO/MXene@PVC membrane demonstrated good lithium ion adsorption with a maximum capacity of 25.4 mg/g. Ge et al. proposed a MXene-based composite membrane by incorporating poly(sodium 4-styrenesulfonate) into MXene for Li^+/Mg^{2+} separation.[15] Abdelrahman et al. reported on hydrogel nanocomposite sorbents containing sulfonated graphene oxide (SGO), MXene, and alginate.[16] The sulfonic acid groups on SGO enable selective lithium ion binding by facilitating Li^+/H^+ exchange while minimizing interference from other ions. Wang et al. fabricated a flexible hybrid film by embedding $MnO_2 \cdot 0.5H_2O$ nanoparticles into a 2D MXene/1D carbon nanofiber structure. The material facilitated rapid lithium ion transport

Received: September 18, 2025
Revised: October 5, 2025
Accepted: October 28, 2025
Published: December 12, 2025

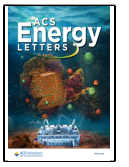

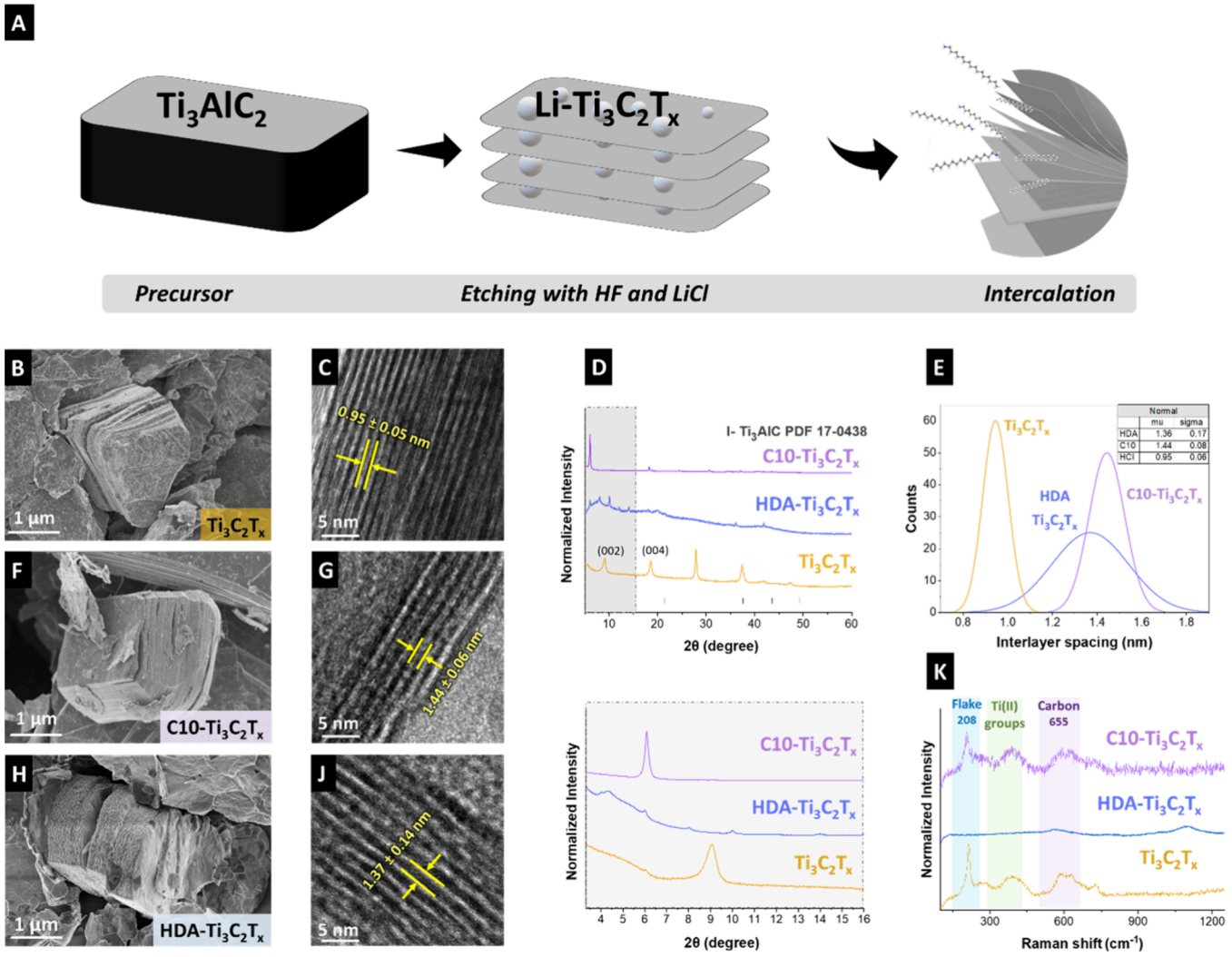

Figure 1. (A) Schematic representation of the synthesis of the MXene. (B–K) Material characterization of $Ti_3C_2T_x$, C10-$Ti_3C_2T_x$, and HDA-$Ti_3C_2T_x$. (B,F,H) Scanning electron micrographs of the materials. (C,G,J) Transmission electron micrographs, (D) X-ray diffractograms. (E) Interlayer spacing values of the materials measured via transmission electron microscopy. (K) Raman spectra.

and enhanced lithium ion selectivity by blocking interfering ions through steric hindrance.[17] In particular, it achieved a sorption capacity of 21.4 mg/g, and lithium ion selectivity (e.g., Li/Na = 29,232 and Li/Mg = 3,606).[17]

Ren et al.[18] employed a hydrogen bond interaction strategy to integrate 2D MXenes as interfacial agents between $Li_{1.33}Mn_{1.67}O_4$ and polysulfone, forming a composite membrane. Their design achieved a high lithium sorption capacity of 21.1 mg/g and stable cycling performance. In 2024, Fahem et al.[13] recovered lithium ions through electrosorption using pseudocapacitive electrodes. Composite materials of polystyrenesulfonated MXene (PM) and a sodium titanate/graphene oxide (NG) were synthesized and applied in a single-cell capacitive deionization system.[13] PM and NG electrodes tested in binary, ternary, and quaternary ionic solutions achieved a lithium ion recovery purity ranging from 59% to 96% and 60% to 77%, respectively.[13] The intercalation of alkylammonium ions into the MXene layers effectively modulates their interlayer spacing and surface chemistry, thereby unlocking new application opportunities for MXenes.[19] Particularly, alkylammonium ion preintercalation leads to the formation of pillars that expand the interlayer spacing, enabling the intercalation of large room-temperature ionic liquid cations and resulting in high energy and power densities in MXene-based supercapacitors.[20]

Although MXene and MXene-based materials exhibit significant potential for lithium ion recovery, research in this area remains limited. To further advance the understanding and efficiency of selective electrochemical lithium ion recovery, our study explored a range of MXene-based materials, with a focus on tunable interlayer spacing. By controlling the interlayer structure, the selective uptake of lithium ions was optimized to enhance the selectivity and overall extraction performance for lithium ion recovery.

Our work highlights the advantages of modifying MXenes with organic molecules for lithium ion extraction. Unlike electrode-level strategies that primarily enhance ion pathways or electrode densities, organic intercalation enables the direct, molecular-level control of interlayer spacing, surface chemistry, and electrostatic environments.[21] This creates selective channels that facilitate lithium ion transport, linking fundamental insights into ion sieving with practical performance and positioning organic-modified MXenes as a highly promising ion-selective material. As illustrated in Figure 1A, a mixture of HF and LiCl was used during the etching process to simultaneously remove Al and intercalate lithium ions between

https://doi.org/10.1021/acsenergylett.5c03009
ACS Energy Lett. 2026, 11, 508–516

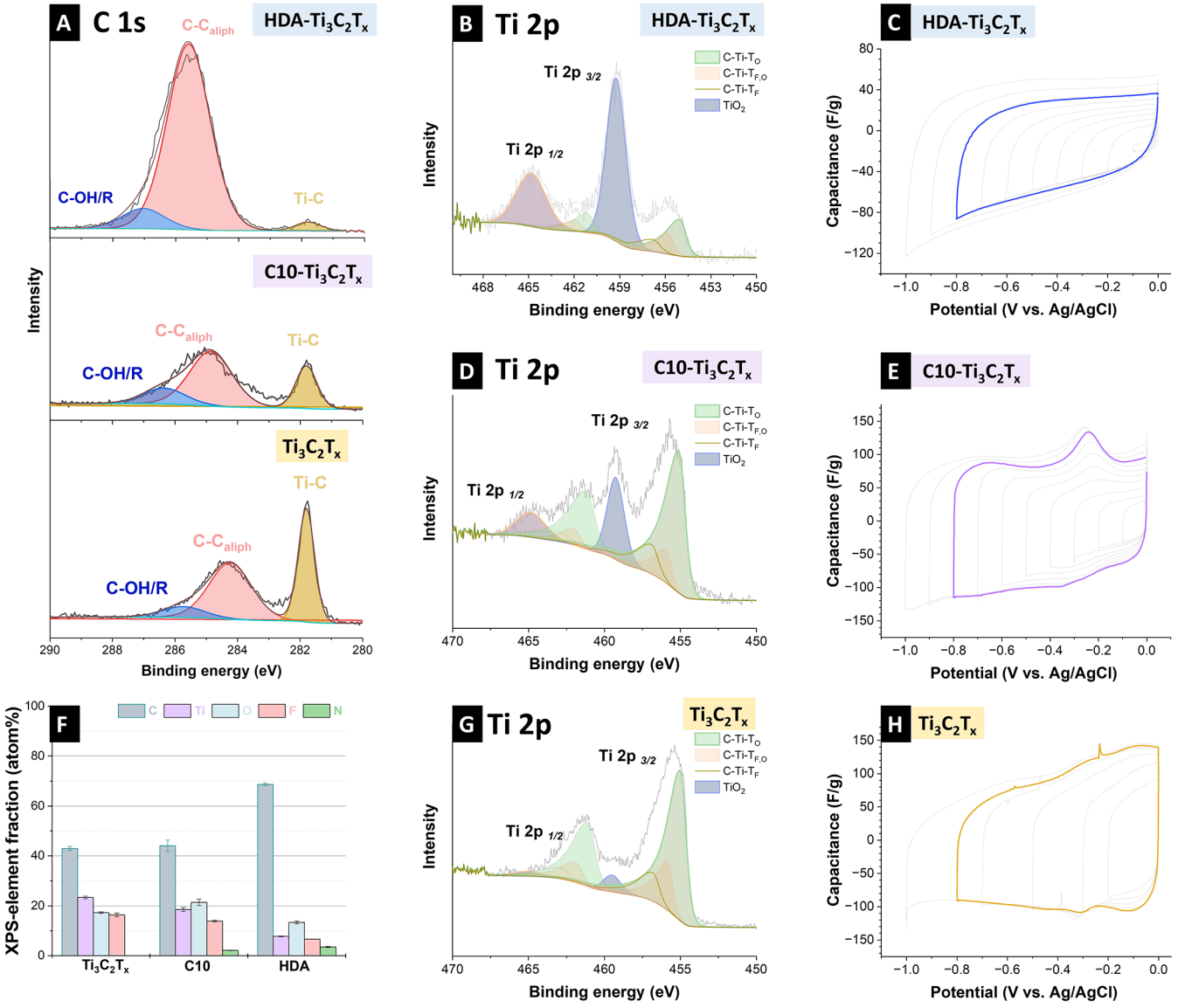

Figure 2. (A-H) Chemical composition and cyclic voltammograms of HDA-$Ti_3C_2T_x$, C10-$Ti_3C_2T_x$, $Ti_3C_2T_x$. (A) Comparison of X-ray photoelectron C 1s spectra. (B,D,G) Highly resolved measured Ti 2p peaks. (F) XPS data-derived elemental composition. (C,E,H) Electrochemical window opening via cyclic voltammetry.

the $Ti_3C_2T_x$ layers. Following etching, cation exchange was achieved by replacing lithium ions with ammonium salts or alkylamines, resulting in an increased interlayer spacing due to the incorporation of long alkyl chains. Figures 1B–J show the morphologies of the multilayered structure of pristine $Ti_3C_2T_x$, C10-$Ti_3C_2T_x$, and HDA-$Ti_3C_2T_x$. X-ray diffractograms of the pristine $Ti_3C_2T_x$, C10-$Ti_3C_2T_x$, and HDA-$Ti_3C_2T_x$ are presented in Figure 1D, where a progressive shift of the (002) reflection to lower angles was observed with increasing intercalant chain length, confirming the expansion of the interlayer spacing (Figure 1E).

Raman spectroscopy showed the presence of the D-band and G-band of incompletely graphitic carbon (Figure 1K).[22] The characteristic signals at 215 cm^{-1}, 394 cm^{-1}, and 605 cm^{-1} correspond to out-of-plane (A_{1g}) and in-plane (E_g) shifts, characteristics of $Ti_3C_2T_x$ MXene flakes, documenting Al removal from the initial MAX phase and the successful synthesis of MXene.[23] The shifts at 394 cm^{-1} were attributed to the E_g of Ti atoms, and the bands at 605 cm^{-1} were in the range of carbon vibrations (A_{1g}-E_g).[24]

X-ray photoelectron survey spectra showed the presence of O, F, Ti, and C at the surface of the samples (Supporting Information, Figure S1). The C10-$Ti_3C_2T_x$ and HDA-$Ti_3C_2T_x$ samples contained additional N and only traces of Cl (Figure 2F). In addition to aliphatically and hydroxidically bound carbon, all C 1s signals showed a distinct peak at a lower binding energy of 281.8 eV, which could be assigned to the carbidic bond (Figure 2A). The highly resolved Ti 2p spectra were fitted with four doublets corresponding to the Ti $2p_{3/2}$ and Ti $2p_{1/2}$ states in Ti-C with different surface terminations (C-Ti-T_O, C-Ti-$T_{F,O}$, C-Ti-T_F), and TiO_2 surroundings, respectively.[25−27] A Shirley background was selected for all peaks. Owing to their conductivity, asymmetric line shapes were employed for the MXene components, whereas a symmetric line shape was used for the oxide.[25] The energetic difference ΔTi 2p, which was due to spin−orbital splitting, was

https://doi.org/10.1021/acsenergylett.5c03009
ACS Energy Lett. 2026, 11, 508−516

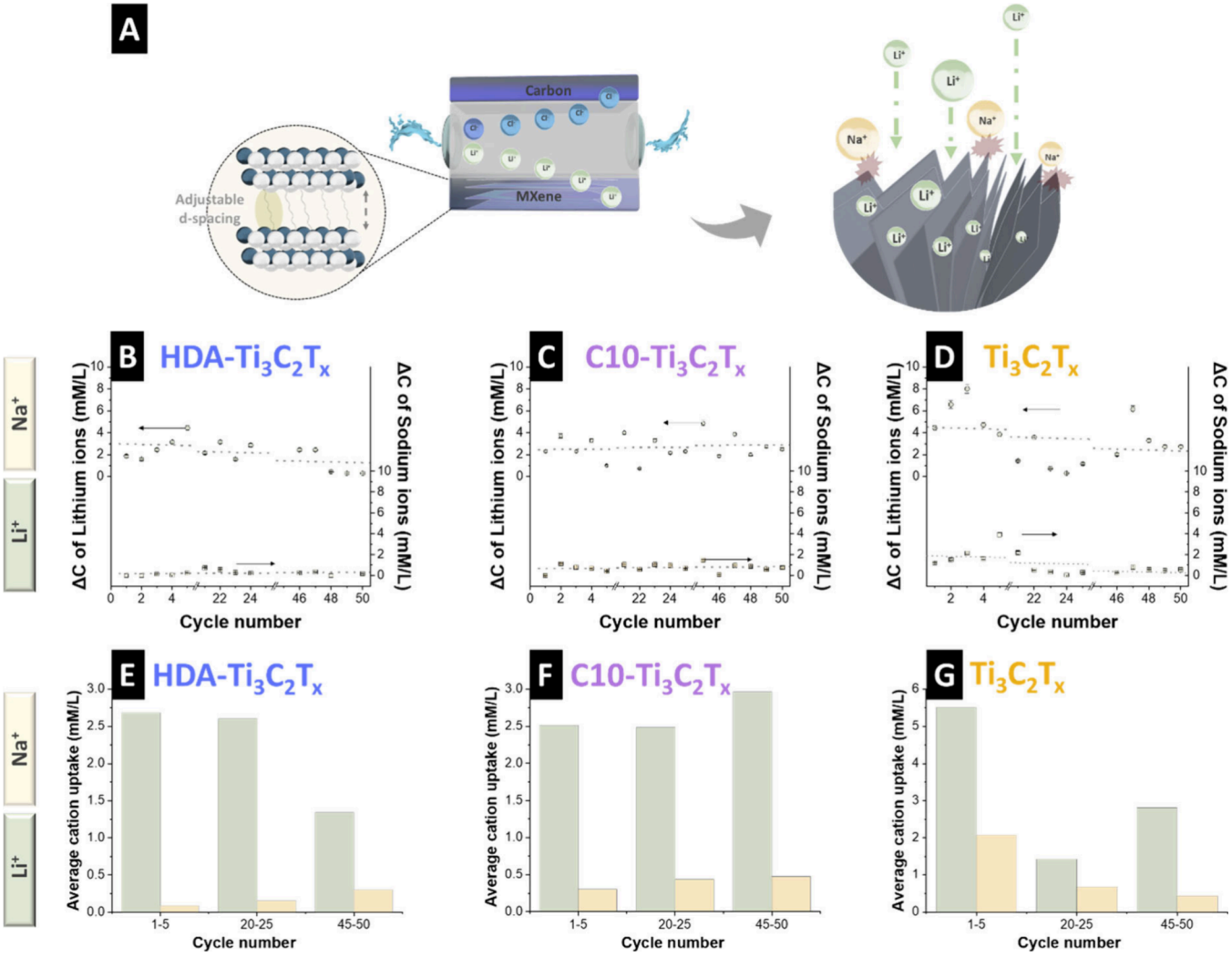

Figure 3. (A) Schematic representation of the electrochemical lithium ion extraction system. Cation uptake of the electrodes for (B) HDA-$Ti_3C_2T_x$, (C) C10-$Ti_3C_2T_x$, and (D) $Ti_3C_2T_x$. Average cation uptake of the electrodes for (E) HDA-$Ti_3C_2T_x$, (F) C10-$Ti_3C_2T_x$, and (G) pristine $Ti_3C_2T_x$.

set to 6.1 eV for the MXene components. For the oxide component, ΔTi 2p was set to 5.6 eV.[25,27]

The Ti $2p_{3/2}$ peak at 459.2 eV was attributed to TiO_2 species. The peaks located at 455.1, 455.9, and 456.9 eV were assigned to C-Ti bonded to O (C-Ti-T_O), C-Ti bonded to both F and O (C-Ti-$T_{F,O}$), and C-Ti bonded only to F (C-Ti-T_F) (Figure 2B-D,G).[28] The Ti 2p spectrum of the pristine sample exhibited the highest carbide content among the analyzed samples (Figure 2G). In contrast, HDA-$Ti_3C_2T_x$ displayed the lowest carbide contribution and the most pronounced presence of TiO_2 (Figure 2B), suggesting that partial surface oxidation occurred during synthesis (Supporting Information, Figure S2). This oxidation was likely facilitated by the relatively elevated synthesis temperature (75 °C) employed in the preparation process of HDA-$Ti_3C_2T_x$.

The N 1s spectra (Supporting Information, Figure S3) provided direct evidence of N-containing species in the C10-$Ti_3C_2T_x$ and HDA-$Ti_3C_2T_x$ samples. The absence of any peaks at 396.5−396.8 eV corresponding to Ti−N confirmed that these N-species were intercalated rather than covalently bonded terminations of the MXene.[29] For C10-$Ti_3C_2T_x$, the N 1s at 402.1 eV corresponded to trimethylammonium group $-N^+(CH_3)_3$. For HDA-$Ti_3C_2T_x$, the additional peak at 401 eV could be attributed to protonated amine species R-NH_3^+.[30] Therefore, both C10 and HDA intercalated as positively charged organic ions, electrostatically interacting with the negatively charged surface of the MXenes while displacing the lithium ions originally present between the MXene layers.[19,31] Evidently, the long alkyl chains stabilized the expanded interlayer spacing, which was consistent with the structural changes observed in the X-ray diffractograms.

Comparative electrochemical data demonstrated that the surface modifications of $Ti_3C_2T_x$ MXene materials influenced their ion selectivity (Figure 2C,E,H). In 1 M NaCl, HDA-$Ti_3C_2T_x$ and C10-$Ti_3C_2T_x$ exhibited higher current responses across various scan rates, indicating faster kinetics than that of pristine $Ti_3C_2T_x$, which showed lower and less symmetric cyclic voltammograms (Supporting Information, Figure S4). In 1 M LiCl, all the samples display increased current densities relative to NaCl, with C10-$Ti_3C_2T_x$ showing prominent redox features, indicating favorable lithium ion intercalation.

The cyclic voltammograms revealed that HDA-$Ti_3C_2T_x$ and C10-$Ti_3C_2T_x$ enhanced lithium ion intercalation over sodium ions in different electrolytes at 1 mV/s, while pristine $Ti_3C_2T_x$ demonstrated a stronger sodium ion response (Supporting Information, Figure S4G-J). This selectivity was attributed to

https://doi.org/10.1021/acsenergylett.5c03009
ACS Energy Lett. 2026, 11, 508−516

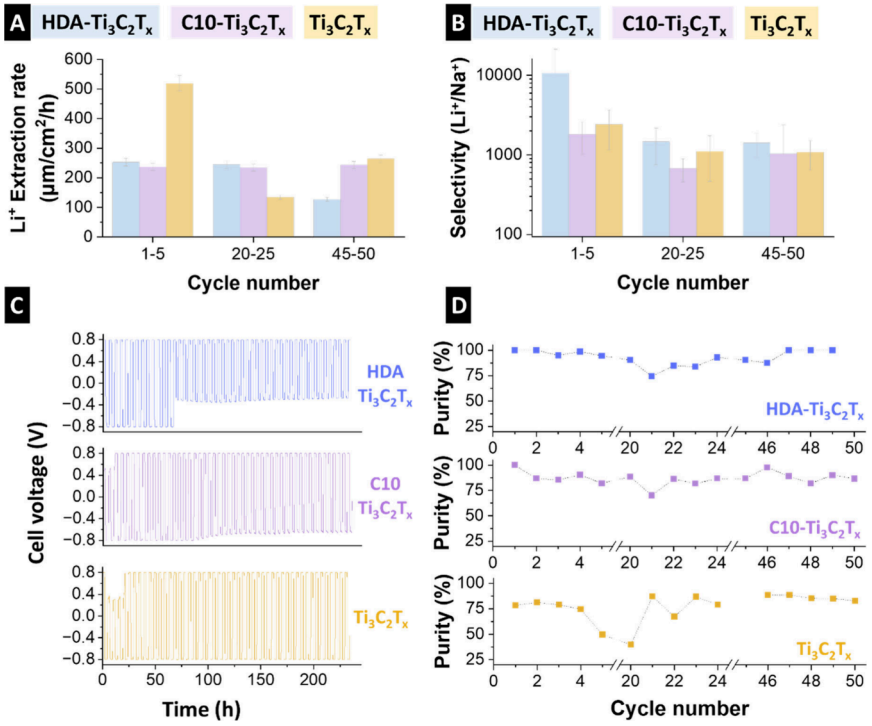

Figure 4. (A) Lithium ion extraction rate of the electrodes. (B) Lithium ion vs sodium ion selectivity of the electrodes. (C) Stability test of the electrodes for operation within −0.8 V to +0.8 V. (D) Purity of the recovery solution.

the electrostatic and coordination interactions between Li ions and the functional groups of the alkyl chains. Owing to their higher charge density and stronger Lewis acidity compared to sodium ions, lithium ions can establish more stable ion-dipole interactions with electron-rich sites along the alkyl chains. In contrast, such interactions are energetically less favorable for sodium ions.[32] The specific capacitance of the three MXene electrodes was evaluated at a scan rate of 1 mV/s over a 0−0.8 V window in 1 M LiCl (Supporting Information, Table S1). HDA-$Ti_3C_2T_x$ and C10-$Ti_3C_2T_x$ yielded capacitances of 37 and 54 F/g, respectively, while the $Ti_3C_2T_x$ sample showed an intermediate capacitance of 23 F/g. Thus, the surface modification and synthesis approach significantly influenced the electrochemical performance.

The two-step lithium ion extraction process is illustrated in Figure 3A. In the first step, the application of an external potential drove lithium ion intercalation while rejecting sodium ions and reversing the potential released lithium ions back into the solution. Figure 3B-D presents the variations in the lithium ion and sodium ion concentrations observed for the different MXene-based electrodes over 50 cycles. HDA-$Ti_3C_2T_x$ stably extracted lithium ions with minimal sodium ion uptake (2.2 mmol/L and 0.18 mmol/L, respectively) (Figure 3B-E). A comparable trend was observed for C10-$Ti_3C_2T_x$; however, a small degree of sodium ion uptake was detected (2.7 mmol/L and 0.4 mmol/L, respectively) (Figure 3C-F). In contrast, the pristine electrode exhibited unstable cycling and the highest lithium ion uptake (3.3 mmol/L) (Figure 3D-G) but with significant sodium ion uptake (1.1 mmol/L), likely due to insufficient control over the interlayer spacing.

Although pristine $Ti_3C_2T_x$ exhibited the highest lithium ion intercalation capacity, it also demonstrated lower selectivity, as evidenced by its substantial sodium ion uptake. Thus, expanding the interlayer spacing through molecular intercalation significantly enhanced the lithium ion selectivity. Among the tested electrodes, HDA-$Ti_3C_2T_x$ and C10-$Ti_3C_2T_x$ exhibited the best performance, combining a high Li-ion uptake with pronounced Na-ion exclusion. These results indicate a compatibility threshold between the solvated ionic diameter and interlayer spacing of the layered materials.[32] Pristine $Ti_3C_2T_x$, with a relatively narrow interlayer spacing of 0.95 nm (9.5 Å), likely restricted the intercalation of solvated ions, thereby limiting the uptake and desorption performance. In contrast, HDA-$Ti_3C_2T_x$ and C10-$Ti_3C_2T_x$, with larger interlayer spacings (1.37 and 1.44 nm, respectively), were more accommodating to solvated ions, potentially enabling more efficient ion diffusion and transport (Figure 1E).

The HDA-$Ti_3C_2T_x$, C10-$Ti_3C_2T_x$, and pristine $Ti_3C_2T_x$ materials showed high Li^+-extraction rates of 207 $\mu m/cm^2/h$, 235 $\mu m/cm^2/h$, and 310 $\mu m/cm^2/h$, respectively (Figure 4A). Although $Ti_3C_2T_x$ had a high initial extraction rate during the first five cycles, its performance declined between cycles 20 and 25, likely because of its unmodified nature. In contrast, the extraction rates of HDA-$Ti_3C_2T_x$ and C10-$Ti_3C_2T_x$ remained relatively stable.

All electrodes exhibited a higher initial Li^+/Na^+ selectivity (Figure 4B) that decreased over time. HDA-$Ti_3C_2T_x$ exhibited the highest early cycle (~10,600) and late-cycle (~1,400) selectivities, confirming the effectiveness of HDA intercalation in favoring Li ions. For comparison, the late-cycle (i.e., cycles 45−50) Li^+/Na^+ selectivities of C10-$Ti_3C_2T_x$ and pristine $Ti_3C_2T_x$ were lower (~1,000). The relatively high selectivity of pristine $Ti_3C_2T_x$ is attributed to the LiCl treatment during synthesis, which preloads lithium ions into the interlayer galleries, effectively templating the structure and lowering the energy barrier for lithium ion insertion or exchange compared to other ions.[33−36] Post-mortem SEM confirmed structural degradation after 50 cycles, particularly for pristine $Ti_3C_2T_x$, where the intercalated structure was no longer visible (Supporting Information, Figure S5). The absence of distinct

https://doi.org/10.1021/acsenergylett.5c03009
ACS Energy Lett. 2026, 11, 508−516

X-ray reflections may indicate a significant expansion in the interlayer spacing beyond the detection limit of XRD used in this study. Alternatively, this could reflect the structural degradation and amorphization of MXene (Supporting Information, Figure S5).[37] The measured increase in the lithium ion extraction rate of pristine $Ti_3C_2T_x$ during cycles 45−50 may be attributed to electrochemically induced interlayer expansion over cycling. Unlike preintercalated materials, which initially benefit from expanded spacing, pristine $Ti_3C_2T_x$ appeared to undergo progressive structural activation, likely owing to gradual Li^+/solvent intercalation. This late-stage expansion enhanced the lithium ion mobility and temporarily improved the purity and extraction rates.

To investigate this phenomenon, we evaluated the electrode stability through extended charge−discharge cycling with the aim of elucidating the correlation between structural degradation and selectivity loss over time (Figure 4C). HDA-$Ti_3C_2T_x$ exhibited a higher degradation rate than the other electrodes. Despite the tailoring effect of long-chain alkylamines, such as HDA, on the MXene structure, their incorporation may introduce trade-offs, including a reduced electrical conductivity, hindered ion transport, and limited electrochemical accessibility owing to the insulating and sterically bulky nature of the organic chains.[7,38] Degradation may also occur by the action of bulk aqueous electrolytes on the interlayer spacing, not just ions. Such a continuous exposure of the interlayer spacing to the aqueous electrolyte may accelerate MXene degradation.

A key challenge in Li extraction is maximizing both the rate and purity, because faster methods often reduce selectivity. The MXene electrodes exhibited both high purity and promising Li-ion extraction capacity (Figure 4D). HDA-$Ti_3C_2T_x$ and C10-$Ti_3C_2T_x$ maintained nearly 100% purity after 50 cycles, whereas the purity of pristine $Ti_3C_2T_x$ significantly decreased to 30% with an unstable performance.

HDA-$Ti_3C_2T_x$ and C10-$Ti_3C_2T_x$ exhibited an average Li^+/Na^+ selectivity of approximately 1500, which is competitive with that of advanced lithium ion selective materials (Table 1). Lithium superionic conductors achieve a higher selectivity (10^4−10^6) but face flux and scalability challenges.[39−41] Diffusion-based methods and LFP electrodes report similar selectivity (900−1000), but with limited recovery or cycling stability.[5] $LiMn_2O_4$ exhibits high diffusion coefficients (10^{-9}−10^{-11} $cm^2 \cdot s^{-1}$), structural stability, and low cost, with optimized electrodes reaching selectivity near 1000.[42] Manganese-based adsorbents also show substantial selectivity (Li^+/Na^+ = 371) in sodium-rich wastewater.[43] Although the HDA-$Ti_3C_2T_x$ selectivity decreased with time, its initial performance rivals or exceeds that of leading membranes and adsorbents, underscoring its potential for practical lithium extraction where both selectivity and durability are important.

Table 1. Lithium-Ion Selectivity Values in This Study Compared to Existing Literature on Advanced Materials

Material	Lithium ion selectivity component	Lithium ion selectivity	Reference
M-T-LIS	adsorbent	674	45
λ-MnO_2	adsorbent	3.4×10^4	46
12-Crown-4 ether	membrane	$(5-1.0) \times 10^2$	47
Spiropyran crown ether	membrane	1.0×10^3	48
Polyamide (PA)	membrane	4.0×10^3	49
$LiTi_2(PO_4)_3$	membrane	ca. 2.6×10^4	39
$Li_{1+x}Al_xGe_{2-x}(PO_4)_3$	membrane	4.1×10^5	5
$Li_{0.33}La_{0.56}TiO_3$ (LLTO)	membrane	4.5×10^7	50
$LiMn_2O_4$/$Li_{1-x}Mn_2O_4$	electrode	1.4×10^3	42
TiO_2-coated $FePO_4$	electrode	1.8×10^4	40
MXene (HDA-$Ti_3C_2T_x$)	electrode	av. 4.5×10^3	This work

This study elucidates the efficacy of interlayer engineering in MXene-based electrodes for the selective extraction of lithium ions using an electrochemical cycling process. The tailored MXenes, particularly those preintercalated with HDA, exhibited an excellent combination of high lithium ion uptake and high sodium ion rejection, outperforming their C10-$Ti_3C_2T_x$ and pristine $Ti_3C_2T_x$ counterparts. The Li^+/Na^+ selectivity observed for HDA-$Ti_3C_2T_x$ highlights the role of alkyl chains in modulating the interlayer chemistry and enhancing ion sieving. Pristine $Ti_3C_2T_x$ exhibited the highest lithium ion uptake but lower selectivity and stability. Long-term cycling revealed a stable performance for C10-$Ti_3C_2T_x$. Conversely, structural degradation was observed for HDA-$Ti_3C_2T_x$, which was attributed to the oxidative instability of bulky organic chains that compromised the electrochemical accessibility and transport kinetics. HDA-$Ti_3C_2T_x$ and C10-$Ti_3C_2T_x$ retained lithium ion purity levels approaching 100% over 50 cycles, in contrast to the 30% decrease observed for pristine MXene. Therefore, interlayer functionalization is an effective strategy for advancing MXene electrodes toward high-rate, high-purity lithium ion extraction, thereby bridging the gap between ion selectivity and operational stability in aqueous electrochemical systems. This way, lithium ion harvesting from natural media[4] or within the context of lithium-ion battery recycling[44] may enable circular applications.[39]

■ ASSOCIATED CONTENT

Data Availability Statement

The data can be made available upon request.

Supporting Information

The Supporting Information is available free of charge at https://pubs.acs.org/doi/10.1021/acsenergylett.5c03009.

Experimental description, details on the material synthesis, XPS survey spectra of the electrodes, *post-mortem* SEM of the electrodes, *post-mortem* XRD of the electrodes, data obtained from cyclic voltammetry, and key performance metrics of the electrodes (PDF)

■ AUTHOR INFORMATION

Corresponding Author

Volker Presser − *INM - Leibniz Institute for New Materials, 66123 Saarbrücken, Germany; Department of Materials Science & Engineering, Saarland University, 66123 Saarbrücken, Germany; saarene, Saarland Center for Energy Materials and Sustainability, 66123 Saarbrücken, Germany;* orcid.org/0000-0003-2181-0590; Email: volker.presser@leibniz-inm.de

Authors

Cansu Kök − *INM - Leibniz Institute for New Materials, 66123 Saarbrücken, Germany; Department of Materials Science & Engineering, Saarland University, 66123 Saarbrücken, Germany*

Karamullah Eisawi − *Department of Physics and Engineering Physics, Tulane University, New Orleans, Louisiana 70118, United States of America;* orcid.org/0000-0002-9031-4809

Jean G. A. Ruthes − *INM - Leibniz Institute for New Materials, 66123 Saarbrücken, Germany; Department of Materials Science & Engineering, Saarland University, 66123 Saarbrücken, Germany;* orcid.org/0000-0001-5262-5932

Burcu Tan − *INM - Leibniz Institute for New Materials, 66123 Saarbrücken, Germany; Department of Materials Science & Engineering, Saarland University, 66123 Saarbrücken, Germany*

Antje Quade − *Leibniz Institute for Plasma Science and Technology (INP), 17489 Greifswald, Germany;* orcid.org/0000-0003-0814-4319

Michael Naguib − *Department of Physics and Engineering Physics, Tulane University, New Orleans, Louisiana 70118, United States of America;* orcid.org/0000-0002-4952-9023

Complete contact information is available at: https://pubs.acs.org/10.1021/acsenergylett.5c03009

Author Contributions

C.K.: methodology, investigation, data curation, validation, writing-original draft. K.E.: investigation, data curation, writing-review and editing. J.G.A.R.: data curation, review and editing. B.T.: data curation, review. A.Q.: data curation, XPS analysis. M.N.: writing-review and editing. V.P.: visualization, writing-review and editing.

Notes

The authors declare no competing financial interest.

■ ACKNOWLEDGMENTS

We acknowledge support for the eLiFlow project from the European Union, specifically the European Regional Development Fund (ERDF), and the State of Saarland, Germany. M.N. acknowledges the support from the Alexander von Humboldt Foundation through the Humboldt Research Award.

■ REFERENCES

(1) (a) Zhang, Y.; Sun, W.; Xu, R.; Wang, L.; Tang, H. Lithium extraction from water lithium resources through green electrochemical-battery approaches: A comprehensive review. *J. Cleaner Prod.* **2021**, *285*, 124905. (b) Vera, M. L.; Torres, W. R.; Galli, C. I.; Chagnes, A.; Flexer, V. Environmental impact of direct lithium extraction from brines. *Nat. Rev. Earth Environ.* **2023**, *4* (3), 149−165.

(2) Farahbakhsh, J.; Arshadi, F.; Mofidi, Z.; Mohseni-Dargah, M.; Kök, C.; Assefi, M.; Soozanipour, A.; Zargar, M.; Asadnia, M.; Boroumand, Y.; et al. Direct lithium extraction: A new paradigm for lithium production and resource utilization. *Desalination* **2024**, *575*, 117249.

(3) (a) Zhao, X.; Yang, H.; Wang, Y.; Sha, Z. Review on the electrochemical extraction of lithium from seawater/brine. *J. Electroanal. Chem.* **2019**, *850*, 113389. (b) Zhu, Q.; Yu, X.; Liu, Y.; Wang, Y.; Yang, P.; Liu, K. Electrochemical lithium extraction with continuous flow electrodes. *Desalination* **2024**, *574*, 117250. (c) Xiong, Y.; Zhou, J.; Lu, P.; Yin, J.; Wang, Y.; Fan, Z. Electrochemical lithium extraction from aqueous sources. *Matter* **2022**, *5* (6), 1760−1791. (d) Battistel, A.; Palagonia, M. S.; Brogioli, D.; La Mantia, F.; Trócoli, R. Electrochemical methods for lithium recovery: A comprehensive and critical review. *Adv. Mater.* **2020**, *32* (23), 1905440.

(4) Kök, C.; Wang, L.; Ruthes, J. G. A.; Quade, A.; Suss, M. E.; Presser, V. Continuous lithium-Ion extraction from seawater and mine water with a fuel cell system and ceramic membranes. *Energy Environ. Mater.* **2024**, *7* (6), No. e12742.

(5) Wang, L.; Arnold, S.; Ren, P.; Wang, Q.; Jin, J.; Wen, Z.; Presser, V. Redox flow battery for continuous and energy-effective lithium recovery from aqueous solution. *ACS Energy Lett.* **2022**, *7* (10), 3539−3544.

(6) (a) VahidMohammadi, A.; Rosen, J.; Gogotsi, Y. The world of two-dimensional carbides and nitrides (MXenes). *Science* **2021**, *372* (6547), No. eabf1581. (b) Pang, J.; Mendes, R. G.; Bachmatiuk, A.; Zhao, L.; Ta, H. Q.; Gemming, T.; Liu, H.; Liu, Z.; Rummeli, M. H. Applications of 2D MXenes in energy conversion and storage systems. *Chem. Soc. Rev.* **2019**, *48* (1), 72−133. (c) Srimuk, P.; Su, X.; Yoon, J.; Aurbach, D.; Presser, V. Charge-transfer materials for electrochemical water desalination, ion separation and the recovery of elements. *Nat. Rev. Mater.* **2020**, *5* (7), 517−538. (d) Xiong, D.; Shi, Y.; Yang, H. Y. Rational design of MXene-based films for energy storage: Progress, prospects. *Mater. Today* **2021**, *46*, 183−211. (e) Naguib, M.; Come, J.; Dyatkin, B.; Presser, V.; Taberna, P.-L.; Simon, P.; Barsoum, M. W.; Gogotsi, Y. MXene: a promising transition metal carbide anode for lithium-ion batteries. *Electrochem. Commun.* **2012**, *16* (1), 61−64. (f) Naguib, M.; Gogotsi, Y. Synthesis of Two-dimensional materials by selective extraction. *Acc. Chem. Res.* **2015**, *48* (1), 128−135.

(7) Naguib, M.; Mashtalir, O.; Carle, J.; Presser, V.; Lu, J.; Hultman, L.; Gogotsi, Y.; Barsoum, M. W. Two-dimensional transition metal carbides. *ACS Nano* **2012**, *6* (2), 1322−1331.

(8) Chen, Z.; Du, J.; Shi, J. Mxene-based lithium-ion sieve polymer membrane for sustainable lithium adsorption. *Sep. Purif. Technol.* **2025**, *354*, 129316.

(9) Lu, Z.; Wu, Y.; Ding, L.; Wei, Y.; Wang, H. A Lamellar MXene (Ti_3C_2T)/PSS composite membrane for fast and selective lithium-Ion separation. *Angew. Chem., Int. Ed.* **2021**, *60* (41), 22265−22269.

(10) Bilibana, M. P. Electrochemical properties of MXenes and applications. *Adv. Sens. Energy Mater.* **2023**, *2* (4), 100080.

(11) Zhao, X.; Zheng, L.; Hou, Y.; Wang, Y.; Zhu, L. Pulsed electric field controlled lithium extraction process by LMO/MXene composite electrode from brines. *Chem. Eng. J.* **2022**, *450*, 138454.

(12) (a) Liu, G.; Xiao, F.; Zhang, T.; Gu, Y.; Li, J.; Guo, D.; Xu, M.; Wu, N.; Cao, A.; Liu, X. In-situ growth of MoO_2@N doped carbon on Mo_2C-MXene for superior lithium storage. *Appl. Surf. Sci.* **2022**, *597*, 153688. (b) Wen, H.; Liu, Z.; Lu, Z.; Yang, Y.; Chen, J. P. High-performance PEI-based nanofiltration membrane by MXene-regulated interfacial polymerization reaction: Design, fabrication and testing. *J. Membr. Sci.* **2025**, *717*, 123568.

(13) Faheem, M.; Alam, R.; Alhajaj, A.; Zou, L. Recovery of lithium by pseudocapacitive electrodes in capacitive deionization. *Electrochim. Acta* **2024**, *489*, 144267.

(14) Li, X.; Chen, L.; Chao, Y.; Zhu, L.; Luo, G.; Sun, J.; Jiang, L.; Zhu, W.; Liu, Z.; Xu, C. Highly selective separation of lithium with hierarchical porous lithium-ion sieve microsphere derived from MXene. *Desalination* **2022**, *537*, 115847.

(15) Ge, M.; Wang, D.; Wei, C.; Liu, S.; Meng, L.; Liu, X.; Fang, T. Insight into the separation mechanisms of MXene@PSS nanochannels for high-efficiency lithium extraction. *Sep. Purif. Technol.* **2025**, *363*, 132082.

(16) Abdelrahman, N. S.; Hong, S.; Choi, D. S.; Arafat, H. A.; AlMarzooqi, F. Interfacial adsorption and recovery of lithium ions using sulfonated graphene oxide and $Ti_3C_2T_x$ MXene nanocomposite hydrogels. *Desalination* **2025**, *606*, 118766.

(17) Wang, M.; Zhang, T.; Meng, Z.; Wang, C.; Dong, W.; Liu, J.; Yang, S.; Hou, X.; Cheng, X.; Liu, W.; et al. Self-intercepting interference of hydrogen-bond induced flexible hybrid film to facilitate lithium extraction. *Chem. Eng. J.* **2023**, *458*, 141403.

(18) Ren, Y.; Zhao, D.; Zhou, F.; Liu, Y.; Fu, C.; Fu, Y.; Gong, T.; Wu, Z.; Yang, X.; Cai, Z. MXene-bridged HMO/PSF adsorptive membrane for selective lithium recovery from shale gas wastewater with suppressed Mn leaching. *Desalination* **2025**, *600*, 118515.

(19) Ghidiu, M.; Kota, S.; Halim, J.; Sherwood, A. W.; Nedfors, N.; Rosen, J.; Mochalin, V. N.; Barsoum, M. W. Alkylammonium cation intercalation into Ti_3C_2 (MXene): Effects on properties and ion-

exchange capacity estimation. *Chem. Mater.* **2017**, *29* (3), 1099−1106.
(20) Liang, K.; Matsumoto, R. A.; Zhao, W.; Osti, N. C.; Popov, I.; Thapaliya, B. P.; Fleischmann, S.; Misra, S.; Prenger, K.; Tyagi, M.; et al. Engineering the interlayer spacing by pre-intercalation for high performance supercapacitor MXene electrodes in room temperature ionic liquid. *Adv. Funct. Mater.* **2021**, *31* (33), 2104007.
(21) (a) Zhang, H.; Zhao, Z.; Wang, Y.; Ni, K.; Wang, Y.; Zhu, L.; Liu, J.; Zhao, X. Structurally engineered solvent-free $LiFePO_4$ electrodes via hot-pressing with efficient ion transport pathways for lithium extraction from brine. *Acta Phys.-Chim. Sin.* **2026**, *42*, 100130. (b) Zhao, X.; Gong, Y.; Gao, K.; Wang, Y.; Yang, H. Y. Tailored LMO@COF composite electrodes for direct electrochemical lithium extraction from high-temperature brines. *Chem. Eng. J.* **2023**, *474*, 145975. (c) Zhao, X.; Wang, Y.; Wang, Y.; Zhang, H.; Zhao, Z.; Zhu, L.; Wang, Y. Integrating flexibility and lattice engineering in AlBr Co-doped self-supporting $LiMn_2O_4$ electrodes for efficient lithium extraction. *Chem. Eng. J.* **2025**, *521*, 166575.
(22) Iqbal, A.; Hamdan, N. M. Investigation and optimization of MXene functionalized mesoporous Titania films as efficient photo-electrodes. *Materials* **2021**, *14* (21), 6292.
(23) Melchior, S. A.; Raju, K.; Ike, I. S.; Erasmus, R. M.; Kabongo, G.; Sigalas, I.; Iyuke, S. E.; Ozoemena, K. I. High-voltage symmetric supercapacitor based on 2D titanium carbide (MXene, Ti_2CT_x)/carbon nanosphere composites in a neutral aqueous electrolyte. *J. Electrochem. Soc.* **2018**, *165* (3), A501−A511.
(24) Sengupta, A.; Rao, B. V. B.; Sharma, N.; Parmar, S.; Chavan, V.; Singh, S. K.; Kale, S.; Ogale, S. Comparative evaluation of MAX, MXene, NanoMAX, and NanoMAX-derived-MXene for microwave absorption and Li ion battery anode applications. *Nanoscale* **2020**, *12* (15), 8466−8476.
(25) Natu, V.; Benchakar, M.; Canaff, C.; Habrioux, A.; Célérier, S.; Barsoum, M. W. A critical analysis of the X-ray photoelectron spectra of $Ti_3C_2T_z$ MXenes. *Matter* **2021**, *4* (4), 1224−1251.
(26) Brette, F.; Célérier, S.; Canaff, C.; Loupias, L.; Paris, M.; Habrioux, A.; Boucher, F.; Mauchamp, V. XPS binding energy shifts in 2D $Ti_3C_2T_z$ MXene go largely beyond intuitive explanations: Rationalization from DFT simulations and experiments. *Small Methods* **2025**, *9* (1), 2400848.
(27) Halim, J.; Cook, K. M.; Naguib, M.; Eklund, P.; Gogotsi, Y.; Rosen, J.; Barsoum, M. W. X-ray photoelectron spectroscopy of select multi-layered transition metal carbides (MXenes). *Appl. Surf. Sci.* **2016**, *362*, 406−417.
(28) Persson, I.; Näslund, L.-Å.; Halim, J.; Barsoum, M. W.; Darakchieva, V.; Palisaitis, J.; Rosen, J.; Persson, P. O. Å. On the organization and thermal behavior of functional groups on Ti_3C_2 MXene surfaces in vacuum. *2D Mater.* **2018**, *5* (1), 015002.
(29) Zhou, C.; Wang, D.; Lagunas, F.; Atterberry, B.; Lei, M.; Hu, H.; Zhou, Z.; Filatov, A. S.; Jiang, D.-e.; Rossini, A. J.; et al. Hybrid organic-inorganic two-dimensional metal carbide MXenes with amido- and imido-terminated surfaces. *Nat. Chem.* **2023**, *15* (12), 1722−1729.
(30) (a) Bruggeman, M.; Zelzer, M.; Dong, H.; Stamboulis, A. Processing and interpretation of core-electron XPS spectra of complex plasma-treated polyethylene-based surfaces using a theoretical peak model. *Surf. Interface Anal.* **2022**, *54* (9), 986−1007. (b) Compton, O. C.; Dikin, D. A.; Putz, K. W.; Brinson, L. C.; Nguyen, S. T. Electrically conductive "alkylated" graphene paper via chemical reduction of amine-functionalized graphene oxide paper. *Adv. Mater.* **2010**, *22* (8), 892−896.
(31) Mashtalir, O.; Lukatskaya, M. R.; Zhao, M.-Q.; Barsoum, M. W.; Gogotsi, Y. Amine-assisted delamination of Nb_2C MXene for Li-ion energy storage devices. *Adv. Mater.* **2015**, *27* (23), 3501−3506.
(32) (a) Ma, J.; Xia, J.; Liang, Z.; Chen, X.; Du, Y.; Yan, C.-H. Layered double hydroxide hollowcages with adjustable layer spacing for high performance hybrid supercapacitor. *Small* **2021**, *17* (49), 2104423. (b) Lian, P.; Dong, Y.; Wu, Z.-S.; Zheng, S.; Wang, X.; Sen, W.; Sun, C.; Qin, J.; Shi, X.; Bao, X. Alkalized Ti_3C_2 MXene nanoribbons with expanded interlayer spacing for high-capacity sodium and potassium ion batteries. *Nano Energy* **2017**, *40*, 1−8. (c) Zhou, Z.; Hong, X.; Ouyang, H.; Xu, P.; Shuai, B.; Wu, X.; Xu, N.; Chen, X.; He, L. Enhanced ion transport in nanochannels of MXenes by Mg^{2+} pre-intercalation. *Phys. Chem. Chem. Phys.* **2022**, *24* (31), 18824−18829.
(33) Tian, C.; Kristiansen, K. R.; Kjelstrup, S.; Barragán, V. M. Two Methods for Determination of Transport Numbers in Ion-Exchange Membranes. *Int. J. Thermophys.* **2022**, *43* (1), 14.
(34) Gurzęda, B.; Boulanger, N.; Nordenström, A.; Dejoie, C.; Talyzin, A. V. Pristine MXene: In situ XRD study of MAX phase etching with HCl+LiF Solution. *Adv. Sci.* **2024**, *11* (48), No. e2408448.
(35) Thakur, A.; Chandran B S, N.; Davidson, K.; Bedford, A.; Fang, H.; Im, Y.; Kanduri, V.; Wyatt, B. C.; Nemani, S. K.; Poliukhova, V.; Kumar, R.; Fakhraai, Z.; Anasori, B. Step-by-Step Guide for Synthesis and Delamination of $Ti_3C_2T_x$ MXene. *Small Methods* **2023**, *7*, 2300030.
(36) Habib, T.; Zhao, X.; Shah, S. A.; Chen, Y.; Sun, W.; An, H.; Lutkenhaus, J. L.; Radovic, M.; Green, M. J. Oxidation stability of $Ti_3C_2T_x$ MXene nanosheets in solvents and composite films. *npj 2D Mater. Appl.* **2019**, *3* (1), 8.
(37) Iakunkov, A.; Boulanger, N.; Gurzeda, B.; Li, G.; Hennig, C.; Svitlyk, V.; Jørgensen, M. R. V.; Kantor, I.; Baburin, I. A.; Hamedi, M. M.; et al. In Situ X-ray Diffraction Study of MXene Synthesis by the Reaction of Ti_3AlC_2 with Molten Zinc and Tin Chlorides. *Chem. Mater.* **2025**, *37* (3), 1132−1142.
(38) Tang, R.; Taguchi, K.; Nishihara, H.; Ishii, T.; Morallón, E.; Cazorla-Amorós, D.; Asada, T.; Kobayashi, N.; Muramatsu, Y.; Kyotani, T. Insight into the origin of carbon corrosion in positive electrodes of supercapacitors. *J. Mater. Chem. A* **2019**, *7* (13), 7480−7488.
(39) Patel, S. K.; Iddya, A.; Pan, W.; Qian, J.; Elimelech, M. Approaching infinite selectivity in membrane-based aqueous lithium extraction via solid-state ion transport. *Sci. Adv.* **2025**, *11* (9), No. eadq9823.
(40) Liu, C.; Li, Y.; Lin, D.; Hsu, P.-C.; Liu, B.; Yan, G.; Wu, T.; Cui, Y.; Chu, S. Lithium extraction from seawater through pulsed electrochemical intercalation. *Joule* **2020**, *4* (7), 1459−1469. acccessed 2025/08/29
(41) Trócoli, R.; Battistel, A.; Mantia, F. L. Selectivity of a Lithium-Recovery Process Based on $LiFePO_4$. *Chem. - Eur. J.* **2014**, *20* (32), 9888−9891.
(42) Guo, Z.-Y.; Ji, Z.-Y.; Wang, J.; Guo, X.-F.; Liang, J.-S. Electrochemical lithium extraction based on "rocking-chair" electrode system with high energy-efficient: The driving mode of constant current-constant voltage. *Desalination* **2022**, *533*, 115767.
(43) Qiu, C.; Luo, X.; Shao, J.; Zhang, H.; Shao, P.; Huang, Y.; Tu, L.; Li, D.; Zhu, W.; Yang, L.; et al. Highly efficient and selective extraction of Li^+ from high sodium lithium containing wastewater using manganese series adsorbent. *J. Hazard. Mater. Adv.* **2023**, *11*, 100347.
(44) Arnold, S.; Ruthes, J. G. A.; Kim, C.; Presser, V. Electrochemical recycling of lithium-ion batteries: Advancements and future directions. *EcoMat* **2024**, *6* (11), No. e12494.
(45) Ding, Y.; Nhung, N. T. H.; An, J.; Chen, H.; Liao, L.; He, C.; Wang, X.; Fujita, T. Manganese-Titanium mixed ion sieves for the selective adsorption of lithium ions from an artificial salt lake brine. *Materials* **2023**, *16* (11), 4190.
(46) Jia-heng, L.; Yong-xi, C.; Qiao-xia, G.; Yu-bin, S.; Jun, Z.; Qi-hua, Y. Preparation of λ-MnO_2 by column method and its ion-sieve property. *J. Wuhan Univ. Technol., Mater. Sci. Ed.* **2002**, *17* (4), 9−12.
(47) Warnock, S. J.; Sujanani, R.; Zofchak, E. S.; Zhao, S.; Dilenschneider, T. J.; Hanson, K. G.; Mukherjee, S.; Ganesan, V.; Freeman, B. D.; Abu-Omar, M. M.; et al. Engineering Li/Na selectivity in 12-Crown-4−functionalized polymer membranes. *Proc. Natl. Acad. Sci. U. S. A.* **2021**, *118* (37), No. e2022197118.
(48) Li, E.; Kang, J.; Ye, P.; Zhang, W.; Cheng, F.; Yin, C. A prospective material for the highly selective extraction of lithium ions

based on a photochromic crowned spirobenzopyran. *J. Mater. Chem. B* **2019**, *7* (6), 903−907.
(49) Peng, Q.; Wang, R.; Zhao, Z.; Lin, S.; Liu, Y.; Dong, D.; Wang, Z.; He, Y.; Zhu, Y.; Jin, J.; et al. Extreme Li-Mg selectivity via precise ion size differentiation of polyamide membrane. *Nat. Commun.* **2024**, *15* (1), 2505.
(50) Li, Z.; Li, C.; Liu, X.; Cao, L.; Li, P.; Wei, R.; Li, X.; Guo, D.; Huang, K.-W.; Lai, Z. Continuous electrical pumping membrane process for seawater lithium mining. *Energy Environ. Sci.* **2021**, *14* (5), 3152−3159.

https://doi.org/10.1021/acsenergylett.5c03009
ACS Energy Lett. 2026, 11, 508−516